

Probing the S2# Subsite of the Anthrax Toxin Lethal Factor Using Novel N-Alkylated Hydroxamates

Elbek K. Kurbanov, Ting-Lan Chiu, Jonathan Solberg, Subhashree Francis, Kimberly M Maize, Jenna Fernandez, Rodney L. Johnson, Jon E. Hawkinson, Michael A. Walters, Barry C. Finzel, and Elizabeth Ambrose Amin

J. Med. Chem., **Just Accepted Manuscript** • DOI: 10.1021/acs.jmedchem.5b01446 • Publication Date (Web): 22 Oct 2015

Downloaded from <http://pubs.acs.org> on October 26, 2015

Just Accepted

“Just Accepted” manuscripts have been peer-reviewed and accepted for publication. They are posted online prior to technical editing, formatting for publication and author proofing. The American Chemical Society provides “Just Accepted” as a free service to the research community to expedite the dissemination of scientific material as soon as possible after acceptance. “Just Accepted” manuscripts appear in full in PDF format accompanied by an HTML abstract. “Just Accepted” manuscripts have been fully peer reviewed, but should not be considered the official version of record. They are accessible to all readers and citable by the Digital Object Identifier (DOI®). “Just Accepted” is an optional service offered to authors. Therefore, the “Just Accepted” Web site may not include all articles that will be published in the journal. After a manuscript is technically edited and formatted, it will be removed from the “Just Accepted” Web site and published as an ASAP article. Note that technical editing may introduce minor changes to the manuscript text and/or graphics which could affect content, and all legal disclaimers and ethical guidelines that apply to the journal pertain. ACS cannot be held responsible for errors or consequences arising from the use of information contained in these “Just Accepted” manuscripts.

Probing the S2' Subsite of the Anthrax Toxin Lethal Factor Using Novel N-Alkylated Hydroxamates

Elbek K. Kurbanov[†], Ting-Lan Chiu[†], Jonathan Solberg[‡], Subhashree Francis[‡],
Kimberly M. Maize[†], Jenna Fernandez[†], Rodney L. Johnson[†], Jon E. Hawkinson[‡],
Michael A. Walters[‡], Barry C. Finzel[†], Elizabeth Ambrose Amin^{†§*}

[†]Department of Medicinal Chemistry, University of Minnesota, Minneapolis, MN 55414; [‡]Institute for Therapeutics
Discovery and Development, University of Minnesota, Minneapolis, MN 55414; [§]Minnesota Supercomputing
Institute for Advanced Computational Research, University of Minnesota, Minneapolis, MN 55455, USA

ABSTRACT

The lethal factor (LF) enzyme secreted by *Bacillus anthracis* is a zinc hydrolase that is chiefly responsible for anthrax-related cell death. Although many studies have been conducted toward the design of small-molecule LF inhibitors, no LF inhibitor is yet available as a therapeutic agent. Inhibitors with considerable chemical diversity have been developed and investigated; however, the LF S2' subsite has not yet been systematically explored as a potential target for lead optimization. Here we present synthesis, experimental evaluation, modeling, and structural biology for a novel series of sulfonamide hydroxamate LF inhibitor analogs specifically designed to extend into, and probe chemical preferences of, this S2' subsite. We discovered that this region accommodates a wide variety of chemical functionalities, and that a broad selection of ligand structural modifications directed to this area can be incorporated without significant deleterious alterations in biological activity. We also identified key residues in this subsite that can potentially be targeted to improve inhibitor binding.

*To whom correspondence should be addressed: eamin@umn.edu

INTRODUCTION

The rod-shaped bacterium *Bacillus anthracis*, the causative agent of anthrax, was disseminated in spore form via the US Postal Service in 2001, resulting in five American deaths.¹ Anthrax continues to pose a significant threat to the public as a biological weapon, and effective postexposure treatments remain elusive. The Centers for Disease Control (CDC) categorizes *B. anthracis* as a Tier 1 Select Agent, a pathogen that poses great risk to national security, economy, and critical infrastructure; this characterization is also due to the fact that the extremely hardy anthrax spores can be weaponized to cause high mortality rates in inhalational form.² Notably, the former Soviet Union and Iraq are rumored to have built aerosolization facilities for the large-scale production of *B. anthracis*.^{3,4} The 1979 anthrax outbreak in Sverdlovsk, in the former Soviet Union, has been attributed to the inhalation of anthrax spores accidentally released at a military microbiological facility in that city.⁵

The lethality of anthrax is largely due to its tripartite exotoxin, comprising lethal factor (LF), a calmodulin-activated adenylate cyclase, edema factor (EF), and protective antigen (PA).⁶ LF, a 89-kDa zinc metalloprotease, is primarily responsible for anthrax pathogenesis, and binds PA to form the anthrax lethal toxin which subsequently enters host target cells.⁷ Once in the cytoplasm, LF cleaves mitogen-activated protein kinase kinases (MAPKKs) MEK1, MEK2, MKK3, MKK4, MKK6, and MKK7.⁸ This leads to the inhibition of MAPK phosphorylation, thereby interfering with cellular immune defense mechanisms.⁷⁻¹² In later stages of the disease, the toxin invades endothelial cells, causing disruption of endothelial barriers and leakage of vasculature, leading to hypovolemia, circulatory shock, and eventual host death.¹³⁻¹⁵ Antibiotics such as fluoroquinolones are effective against *B. anthracis*, but they must be administered early in the disease cycle due to rapid exotoxin secretion. Unfortunately, diagnosis of anthrax in its

1
2
3 early stages poses major challenges, as symptoms of infection are often nonspecific.¹⁶ In later
4 stages of the disease course, antibiotics may yet clear the bacilli, but high levels of toxin can
5 remain systemically and cause fatal residual toxemia. The current arsenal of available antibiotics,
6 of course, has no effect on the LF toxin itself.
7
8
9
10
11

12 Other treatment options include antibody-based therapeutics, which exhibit their own set
13 of limitations. Antibody-based treatments belong to a well-established drug class that has a fairly
14 high success rate for clinical approval, and are usually well tolerated by humans, but key caveats
15 exist: they are very expensive due to the high cost of manufacturing and the often large doses
16 required; also, rare but serious adverse effects have been reported. Antibodies can display
17 significant pharmacokinetic liabilities, limited tissue accessibility, and impaired interactions with
18 the immune system.^{17,18} Consistent with antibody-based target restriction to those on the surface
19 or exterior of host cells, all anti-anthrax antibodies developed to date target the protective antigen
20 in order to interfere with LF translocation into host cells. One of the first fully human
21 monoclonal antibodies developed was MDX-1303, which has now been incorporated into the
22 CDC Strategic National Stockpile (SNS). However, post-exposure studies performed on non-
23 human primates (NHPs) showed that MDX-1303 could only achieve 70% efficacy.¹⁹ In 2012,
24 the Food and Drug Administration (FDA) approved raxibacumab in combination with antibiotics
25 for the treatment of inhalational anthrax. Raxibacumab is a recombinant human immunoglobulin
26 G1 λ monoclonal antibody that prevents binding of PA to cell surfaces. Despite achieving FDA
27 approval, efficacy studies performed on *Cynomolgus* macaques and New Zealand white (NZW)
28 rabbits showed that raxibacumab is inferior to currently approved antimicrobials.^{20,21}
29
30
31
32
33
34
35
36
37
38
39
40
41
42
43
44
45
46
47
48
49
50
51
52

53 More recently, the FDA approved Anthrax Immune Globulin Intravenous (Human), a
54 purified human immune globulin G in combination with antibiotics to treat patients with
55
56
57
58
59
60

1
2
3 inhalational anthrax. Its mechanism of action is similar to that of raxibacumab. Efficacy studies
4
5 performed with *Cynomolgus* macaques and NZW rabbits demonstrated that even in combination
6
7 with antimicrobials, complete protection of animals from *B. anthracis* by Anthrax Immune
8
9 Globulin Intravenous (Human) remains challenging.²² Overall, for post-exposure anthrax
10
11 treatment, there is still a key unmet need for novel therapeutics that reliably and effectively
12
13 protect against the direct effects of the anthrax toxin itself. Given the critical role of LF in
14
15 anthrax pathogenesis and lethality, the discovery of strategies to inhibit this enzyme is still the
16
17 most promising approach to combat post-exposure anthrax.^{23,24}
18
19
20
21

22 The lethal factor consists of four domains: the N-terminal domain (I), a large central
23
24 domain (II), a small helical domain (III), and the C-terminal catalytic domain (IV).²⁵ The N-
25
26 terminal domain (I) (residues 1-263), binds to PA and is responsible for enabling LF
27
28 translocation into host cells. The functions of domains II (residues 264-297 and 385-550) and III
29
30 (residues 303-382) are not fully understood; however, it is known that domain III plays an
31
32 important role in terms of LF selectivity for MAPKKs. The C-terminal domain IV (residues 552-
33
34 776) contains the LF active site, which features a catalytic Zn²⁺ coordinated to three active site
35
36 residues: His686, His690, and Glu735. Residues His686 and His690 form part of the signature
37
38 HEXXH consensus motif that is characteristic of most matrix metalloproteinases (MMPs) as
39
40 well as of other related Zn-binding enzymes.^{25,26}
41
42
43
44
45

46 Numerous studies have been conducted toward the design of small molecule LF
47
48 inhibitors.²⁷⁻³⁶ The first reported LF inhibitors were small peptide sequences, designed as mimics
49
50 of the natural MAPKK substrate, chemically linked to hydroxamic acid zinc-binding groups
51
52 (ZBGs).³⁷⁻³⁹ However, their development as therapeutic agents has been limited because of the
53
54 pharmacokinetic and toxicological liabilities of hydroxamates. Recent research has therefore
55
56
57
58
59
60

1
2
3 focused on the development of non-hydroxamate-based LF inhibitors.^{24,28–32,40–51} Reported
4 inhibitors have included cationic polyamines,³⁰ aminoglycosides,⁴¹ pyrazolones,³¹ polyphenols,⁴⁷
5
6 tetracyclins,⁴² α -defensins,⁴⁸ quinolines,⁴⁰ rhodanines,⁴³ and catechols²⁴ with most of these
7
8
9
10 compounds exhibiting low- to mid-micromolar activity against LF.

11
12
13 The LF active site consists of three prominent subsites: a strongly hydrophobic and
14
15 sterically constrained S1' subsite, a mostly hydrophobic but less sterically restricted, open-ended
16
17 S1-S2 region that forms a solvent-exposed groove, and the less well characterized, flexible S2'
18
19 area (Figures 1a and 1b). The S1' and S1-S2 subsites have been previously explored and well
20
21 characterized in the literature.^{27,33} Our pharmacophore map assembly **UM1**⁵² (Figure 2a)
22
23 reported earlier includes features representing interactions involving all three subsites of the LF
24
25 catalytic binding region, but due to the general dearth of inhibitors targeting the S2' subsite, our
26
27 assembly only partly explores that area. Importantly, **UM1** only incorporated features interacting
28
29 with Lys656 at the entrance of the S2' subsite, and did not include any interactions located
30
31 beyond this entry region (Figure 2b). Therefore, although our pharmacophore hypothesis defined
32
33 part of the S2' region, it remained to be established whether residues deeper within the S2'
34
35 subsite were capable of influencing LF inhibitory activities.

36
37
38
39
40
41 In order to more thoroughly explore this sub-region, we synthesized and experimentally
42
43 evaluated a series of novel LF inhibitors based on existing scaffolds, in order to explore deeper
44
45 regions of the S2' subsite, and thereby identify residues in that area, if any, that play critical roles
46
47 in LF inhibition. Upon examining the published X-ray structure of the Merck sulfonamide
48
49 hydroxamate compound **13** (**MK-702/LF1-B**) (Figure 3) co-crystallized with LF (PDB ID:
50
51 1YQY),^{27,50} it was noted that the S2' subsite could be reached by means of substitutions
52
53
54
55 extending from the sulfonamide nitrogen. We therefore designed and synthesized a series of **13**
56
57
58
59
60

1
2
3 and related (compound **3r** (MK-31)²⁷) derivatives functionalized at that nitrogen, and thereby
4
5 uncovered key design principles and pinpointed previously unidentified ligand-receptor
6
7 interactions in the S2' subsite. It is important to note that our goal in the work reported here was
8
9 not to design a new series of potential therapeutics per se, nor necessarily to increase compound
10
11 potency over the parent compound in this particular series. Our objective, rather, was to
12
13 construct a series of probe compounds based on a known LF inhibitor scaffold with well
14
15 characterized binding modes, in order to explore practical boundaries of this subsite and identify
16
17 preferred contact points for favorable intermolecular interactions. Such information could then
18
19 be applied to the design and optimization of novel LF inhibitors based on non-hydroxamate or
20
21 other types of scaffolds.
22
23
24
25
26
27
28

29 RESULTS

30 Structural Biology, Modeling, and Synthesis

31
32
33
34 Compound **3r** (Table 1), an analog of **13** with the tetrahydropyranyl group replaced by a
35
36 methyl moiety, was selected as the scaffold for initial analog enumeration due to synthetic
37
38 tractability and functionalizability at the sulfonamide nitrogen. In order to confirm previously
39
40 reported inhibition by this compound and to affirm that its binding mode could be accurately
41
42 predicted, **3r** was re-synthesized and a crystal structure in complex with the N-terminally
43
44 truncated LF enzyme was determined at 2.65 Å resolution by X-ray crystallography. Diffraction
45
46 statistics are summarized in Supporting Information. We found that this compound binds as
47
48 predicted from analysis of the **13** complex structure: the hydroxamate coordinates to the Zn²⁺
49
50 cation co-factor, the fluoromethylbenzyl group directs into the S1' pocket between Leu677,
51
52 His686 and Tyr728, and the sulfonamide oxygen engages in H-bonds with backbone amides of
53
54
55
56
57
58
59
60

1
2
3 Lys656 and Gly657. Also as in the complex with **13**, the sulfonamide NH makes a H-bond with
4 the OH of Tyr728, and is in contact with an aspartic acid (Asp328) reaching across the inhibitor
5 binding groove from domain III (Figure 4a).
6
7
8
9

10 To confirm that analogs of **3r** alkylated at the sulfonamide nitrogen continue to inhibit
11 LF, compound **3a** was prepared and characterized (Table 1). This analog, with only a methyl
12 group attached to the sulfonamide N, is expectedly less potent (LF IC₅₀ = 37 μM) than the parent
13 compound, but crystallographic analysis confirms that its binding mode is similar to that of **3r**
14 (Figure 4b). This loss in potency is attributable to the disruption of important hydrogen bonds
15 involving the sidechain OH of Tyr728, as well as to the non-bonded strain introduced into the
16 system upon **3a** binding. Specifically, removal of a hydrogen bond donor at the ligand
17 sulfonamide eliminates a key hydrogen bond to Tyr728, and the hydroxyl moiety moves
18 approximately 0.8 Å in response to the increased steric bulk of the methyl group. In the novel
19 analog, residue Tyr728 does preserve a hydrogen bond with the hydroxamate carbonyl, but an
20 additional hydrogen bond to Asp328 found in the **3r** and **13** complexes is eliminated. This loss of
21 this H-bond does not appear to be sufficient to induce domain III movement, as the complex with
22 **3a** remains in the tight conformation exhibited by X-ray structures of the **13** and **3r** complexes
23 (see below). A sulfonamide methyl or methylene can fit within this severely constrained
24 environment, whereas bulkier branched substituents such as the isopropyl of **3q** cannot fit, and
25 consequently retain no activity (Table 1).
26
27
28
29
30
31
32
33
34
35
36
37
38
39
40
41
42
43
44
45
46
47

48 Preliminary modeling based upon the **3r** complex structure led to the synthesis and
49 evaluation of a series of compounds with a benzyl moiety substituting for the methyl of **3a** as
50 described earlier.⁵³ While these compounds resulted in only marginal increases in potency over
51 **3a**, crystal structures with five of these analogs revealed key structural information, namely, the
52
53
54
55
56
57
58
59
60

1
2
3 extent to which LF is capable of dynamic adaptation in conformation in response to ligand
4 binding. These structures confirmed that the benzyl substituent occupies the S2' site, but also
5 illustrate that movement of domain III can dramatically expand S2'. A second conformation
6 (which we call "open") was observed with some inhibitors that exposes crucial residues such as
7 Asp328, Lys380, and His654 to ligand binding, offering multiple potential sites for favorable
8 charge-charge and H-bonding interactions between ligand and protein. However, specific
9 identification of particular ligand features that influence conformational state was not possible
10 from the study of these compounds; therefore, a larger empirical exploration of more diverse
11 analogs was initiated.

12
13
14
15
16
17
18
19
20
21
22
23
24
25 An exhaustive docking and scoring validation analysis was first conducted that
26 established Glide 5.9⁵⁴⁻⁵⁷ as the most suitable virtual screening package for the LF system from
27 among a series of commercially available docking algorithms. We found that Glide 5.9
28 performed superior to Surflex-Dock,^{58,59} Glide,⁵⁴⁻⁵⁷ AutoDock,⁶⁰ and MOE⁶¹ (see Supporting
29 Information for data and analysis), as assessed by RMSD values between experimental and
30 docked ligand configurations. To select the most appropriate receptor structures for docking, we
31 cross-docked the five co-crystallized ligands into each of the five protein structures published in
32 Ref. 53. Structures 4PKS and 4PKV were selected for further docking studies since these
33 complexes exhibited the lowest ligand RMSD values, 0.91 Å and 0.93 Å respectively, between
34 experimental and predicted bound configurations. Glide 5.9 was therefore chosen to carry out all
35 subsequent docking experiments.

36
37
38
39
40
41
42
43
44
45
46
47
48
49
50
51 To begin the evaluation of new **3r** analogs, an *in silico* library was designed from three
52 Sigma-Aldrich structure sets of aliphatic bromides, benzyl bromides and aliphatic iodides.
53
54
55
56
57
58
59
60
61
62
63
64
65
66
67
68
69
70
71
72
73
74
75
76
77
78
79
80
81
82
83
84
85
86
87
88
89
90
91
92
93
94
95
96
97
98
99
100
101
102
103
104
105
106
107
108
109
110
111
112
113
114
115
116
117
118
119
120
121
122
123
124
125
126
127
128
129
130
131
132
133
134
135
136
137
138
139
140
141
142
143
144
145
146
147
148
149
150
151
152
153
154
155
156
157
158
159
160
161
162
163
164
165
166
167
168
169
170
171
172
173
174
175
176
177
178
179
180
181
182
183
184
185
186
187
188
189
190
191
192
193
194
195
196
197
198
199
200
201
202
203
204
205
206
207
208
209
210
211
212
213
214
215
216
217
218
219
220
221
222
223
224
225
226
227
228
229
230
231
232
233
234
235
236
237
238
239
240
241
242
243
244
245
246
247
248
249
250
251
252
253
254
255
256
257
258
259
260
261
262
263
264
265
266
267
268
269
270
271
272
273
274
275
276
277
278
279
280
281
282
283
284
285
286
287
288
289
290
291
292
293
294
295
296
297
298
299
300
301
302
303
304
305
306
307
308
309
310
311
312
313
314
315
316
317
318
319
320
321
322
323
324
325
326
327
328
329
330
331
332
333
334
335
336
337
338
339
340
341
342
343
344
345
346
347
348
349
350
351
352
353
354
355
356
357
358
359
360
361
362
363
364
365
366
367
368
369
370
371
372
373
374
375
376
377
378
379
380
381
382
383
384
385
386
387
388
389
390
391
392
393
394
395
396
397
398
399
400
401
402
403
404
405
406
407
408
409
410
411
412
413
414
415
416
417
418
419
420
421
422
423
424
425
426
427
428
429
430
431
432
433
434
435
436
437
438
439
440
441
442
443
444
445
446
447
448
449
450
451
452
453
454
455
456
457
458
459
460
461
462
463
464
465
466
467
468
469
470
471
472
473
474
475
476
477
478
479
480
481
482
483
484
485
486
487
488
489
490
491
492
493
494
495
496
497
498
499
500
501
502
503
504
505
506
507
508
509
510
511
512
513
514
515
516
517
518
519
520
521
522
523
524
525
526
527
528
529
530
531
532
533
534
535
536
537
538
539
540
541
542
543
544
545
546
547
548
549
550
551
552
553
554
555
556
557
558
559
560
561
562
563
564
565
566
567
568
569
570
571
572
573
574
575
576
577
578
579
580
581
582
583
584
585
586
587
588
589
590
591
592
593
594
595
596
597
598
599
600
601
602
603
604
605
606
607
608
609
610
611
612
613
614
615
616
617
618
619
620
621
622
623
624
625
626
627
628
629
630
631
632
633
634
635
636
637
638
639
640
641
642
643
644
645
646
647
648
649
650
651
652
653
654
655
656
657
658
659
660
661
662
663
664
665
666
667
668
669
670
671
672
673
674
675
676
677
678
679
680
681
682
683
684
685
686
687
688
689
690
691
692
693
694
695
696
697
698
699
700
701
702
703
704
705
706
707
708
709
710
711
712
713
714
715
716
717
718
719
720
721
722
723
724
725
726
727
728
729
730
731
732
733
734
735
736
737
738
739
740
741
742
743
744
745
746
747
748
749
750
751
752
753
754
755
756
757
758
759
760
761
762
763
764
765
766
767
768
769
770
771
772
773
774
775
776
777
778
779
780
781
782
783
784
785
786
787
788
789
790
791
792
793
794
795
796
797
798
799
800
801
802
803
804
805
806
807
808
809
810
811
812
813
814
815
816
817
818
819
820
821
822
823
824
825
826
827
828
829
830
831
832
833
834
835
836
837
838
839
840
841
842
843
844
845
846
847
848
849
850
851
852
853
854
855
856
857
858
859
860
861
862
863
864
865
866
867
868
869
870
871
872
873
874
875
876
877
878
879
880
881
882
883
884
885
886
887
888
889
890
891
892
893
894
895
896
897
898
899
900
901
902
903
904
905
906
907
908
909
910
911
912
913
914
915
916
917
918
919
920
921
922
923
924
925
926
927
928
929
930
931
932
933
934
935
936
937
938
939
940
941
942
943
944
945
946
947
948
949
950
951
952
953
954
955
956
957
958
959
960
961
962
963
964
965
966
967
968
969
970
971
972
973
974
975
976
977
978
979
980
981
982
983
984
985
986
987
988
989
990
991
992
993
994
995
996
997
998
999
1000

1
2
3 excluded from the set. Interactive enumeration in Maestro was used to computationally generate
4
5 90 synthetically tractable analogs of **3r**. All 90 structures were docked using the Glide XP
6
7 protocol in the Schrödinger Maestro Discovery Suite 9.4 (Schrödinger, Inc.) into the PDB
8
9 structure 4PKR (obtained by us), the best representative LF complex adopting the open
10
11 conformation. Docking and scoring revealed that incorporating polar functionalities such as
12
13 amino, amido, or carboxyl groups into the *N*-alkylating substituent allows for favorable charge-
14
15 charge interactions with the side chains of Lys380 and Asp328, as well as H-bonding
16
17 interactions with the backbone of His654 and Asp328. We then proceeded to design and
18
19 synthesize an extended library of **3r** analogs incorporating polar functionalities based on our
20
21 docking results (Table 1).
22
23
24
25
26

27 Complexes with inhibitors **5a** (5D1T) and **5c** (5D1U) were also characterized
28
29 crystallographically by our team. These inhibitors do induce the open conformation of LF which,
30
31 as reported by us previously, is characterized by an extended distance between domain III and
32
33 the catalytic center, and by a larger hinge angle.⁵³ We believe this can be attributed to the bulk of
34
35 the *N*-alkylation that cannot be accommodated within the smaller confines of S2' in the tight LF
36
37 conformation. In this previous work,⁵³ a *meta*-substituted benzylated **3r** derivative was reported
38
39 (PDB ID 4PKU), wherein the benzyl was found to adopt a unique orientation within the S2'
40
41 subsite, possibly due to the substitution pattern. However, in complex with **5a**, it is evident that
42
43 *meta*-substitution is not sufficient to cause this change; in this structure, the standard position of
44
45 the S2' component is observed. Importantly, structure 5D1U represents the only successfully LF-
46
47 crystallized compound (**5c**) with an extended aliphatic chain. Note that while the *N*-substituent of
48
49 this compound is only ordered through the first three carbons (see Supporting Information), this
50
51 moiety clearly occupies the S2' subsite.
52
53
54
55
56
57
58
59
60

1
2
3
4
5
6
7
8
9
10
11
12
13
14
15
16
17
18
19
20
21
22
23
24
25
26
27
28
29
30
31
32
33
34
35
36
37
38
39
40
41
42
43
44
45
46
47
48
49
50
51
52
53
54
55
56
57
58
59
60

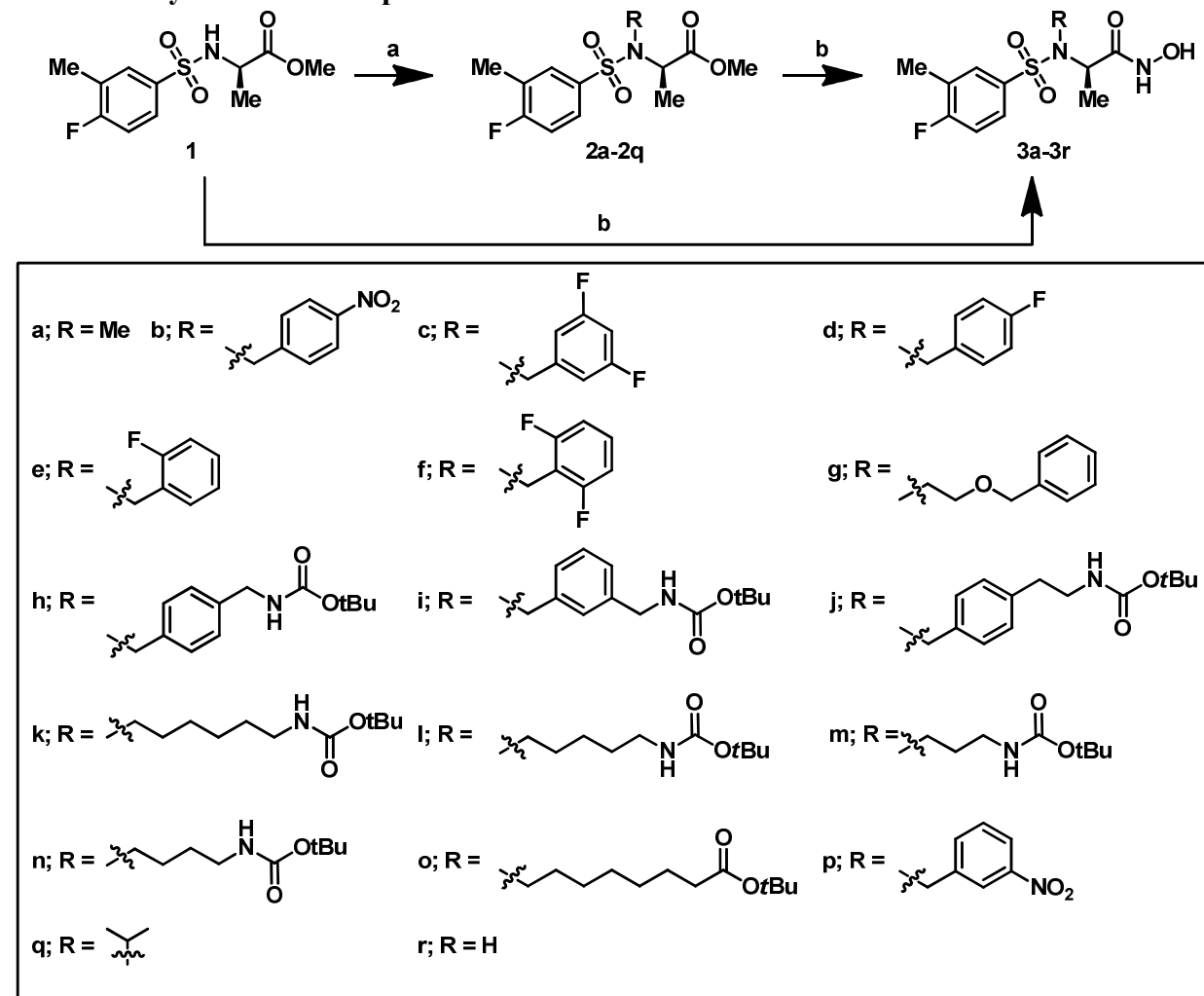
Based on previous studies,⁵³ it was expected that the stabilization of domain III in the tight position would be advantageous for potent inhibitors, as this domain configuration is observed both when no ligand is bound and when the potent inhibitors **13** or **3r** (PDB ID: 4WF6) are co-crystallized with LF. However, three LF X-ray co-crystal structures that we have just deposited -- with **3a** (5D1S), **5a** (5D1T), and **5c** (5D1U) -- demonstrate that this is not always the case. Structures 5D1T, a complex with compound **5a**, and 5D1U, a complex with compound **5c**, present with domain III in the open position, yet the co-crystallized ligands are among the more potent analogs tested. While the primary amine functionality is not well resolved in either of these structures, it is clear that these ligands induce the open rather than the tight configuration of the protein. The co-crystallized compound in 4PKT, on the other hand, induces the tight position without enhancement of activity, as opposed to the co-crystallized compound in 4PKR which induces the open position.⁵³ From these studies, we have concluded that inhibitors are not necessarily required to induce the tight conformation of LF in order to achieve favorable potency; rather, the position of domain III is more closely correlated with the size and substitution pattern at the sulfonamide N on the ligand. The open position is observed when a large substitution or non-*para* benzylation is introduced, and the tight position is manifested when the substitution is small or when benzylation is *p*-substituted (as in 4PKT and 4PKV), as the latter is too large and inflexible to be accommodated by the open position of domain III. Interestingly, with a *p*-substituted benzylation, the S-N-C α -C β torsion angle is decreased, allowing domain III to once again occupy the tight configuration.

Chemistry

Synthetic modifications to the **3r** sulfonamide were accomplished from advanced intermediate **1**, the synthesis of which was previously reported by our laboratory.⁵³ Intermediate **1** was alkylated using various bromides and K₂CO₃ in DMF to give **2a-2p** in 52%-88% yield (**Scheme 1a**). Intermediate **2q** was preferentially alkylated under Mitsunobu conditions employing 2-propanol, PPh₃, and DIAD, which increased the yield to 54% (from 17% with the S_N2 methodology). Esters **1** and **2a-2q** were converted to their corresponding hydroxamic acids **3a-3r** using hydroxylamine hydrochloride and NaOMe in MeOH in 27% – 87% yield (**Scheme 1b**). **3b** was further hydrogenated to **4a** using 10% wt. Pd/C in 43% yield. Compounds **3i-3o** were deprotected using 4 N HCl in 1,4-dioxane or a solution of TFA/DCM (1:2) to their corresponding hydrochloride or trifluoroacetate salts **5a-5g** (**Scheme 2**). Acetylated analogues **7a-7f** were synthesized by means of a three-step procedure from **2h-2m** (**Scheme 3**). Initially, Boc-protected intermediates **2h-2m** were deprotected using 4 N HCl in 1,4-dioxane, and the resulting amines were acetylated with Ac₂O, TEA, and DMAP to give **6a-6f** in 33%-95% yield. Finally, the penultimate esters were converted to their corresponding hydroxamic acids using hydroxylamine hydrochloride and NaOMe in MeOH as described above. Methyl amide **9** was synthesized in parallel fashion over three steps (**Scheme 4**). Initially, *t*Bu-ester **2o** was deprotected with TFA/DCM (1:3). The resulting carboxylic acid was coupled with methylamine hydrochloride using EDCI, HOBt, and NMM to yield methyl ester **8** in 71% yield. The desired hydroxamate was accomplished using the previously described procedure in 30% yield. Compound **12** was synthesized according to **Scheme 5**. The *m*-nitrobenzyl substituent was first hydrogenated to the *m*-amine using 10% wt. Pd/C in MeOH in 77% yield. The free amine was

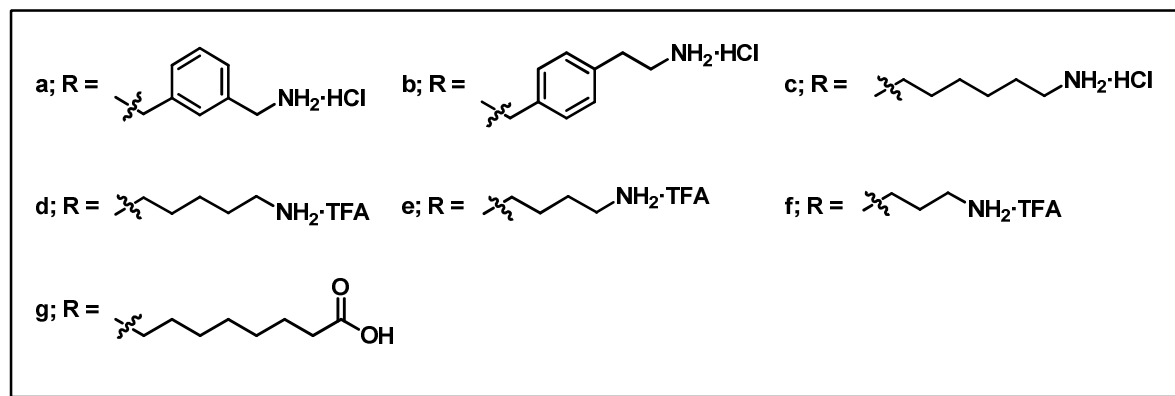
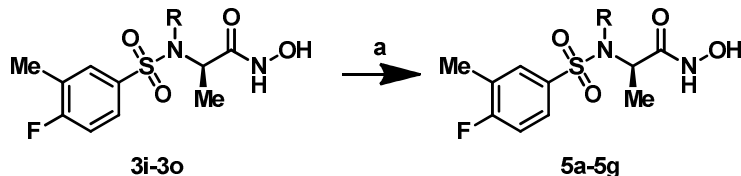
acetylated with AcCl to yield **11**, which was subsequently converted to hydroxamic acid **12** under the previously described conditions.

Scheme 1. Synthesis of Compounds 3a-3r.



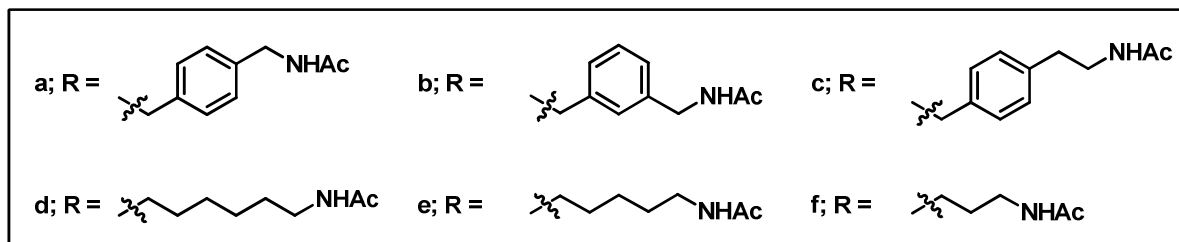
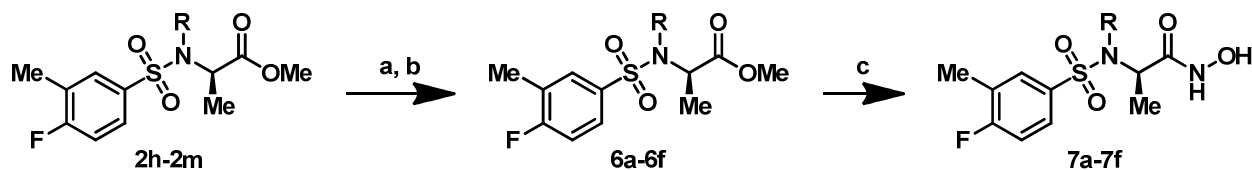
Reagents and Conditions: (a) R-Br, K₂CO₃, DMF, rt, 2 days; for **2q**: 2-propanol, PPh₃, DIAD, THF (b) NH₂OH·HCl, NaOMe, MeOH, 0 °C to rt, 16 h.

Scheme 2. Synthesis of Compounds 5a-5g.



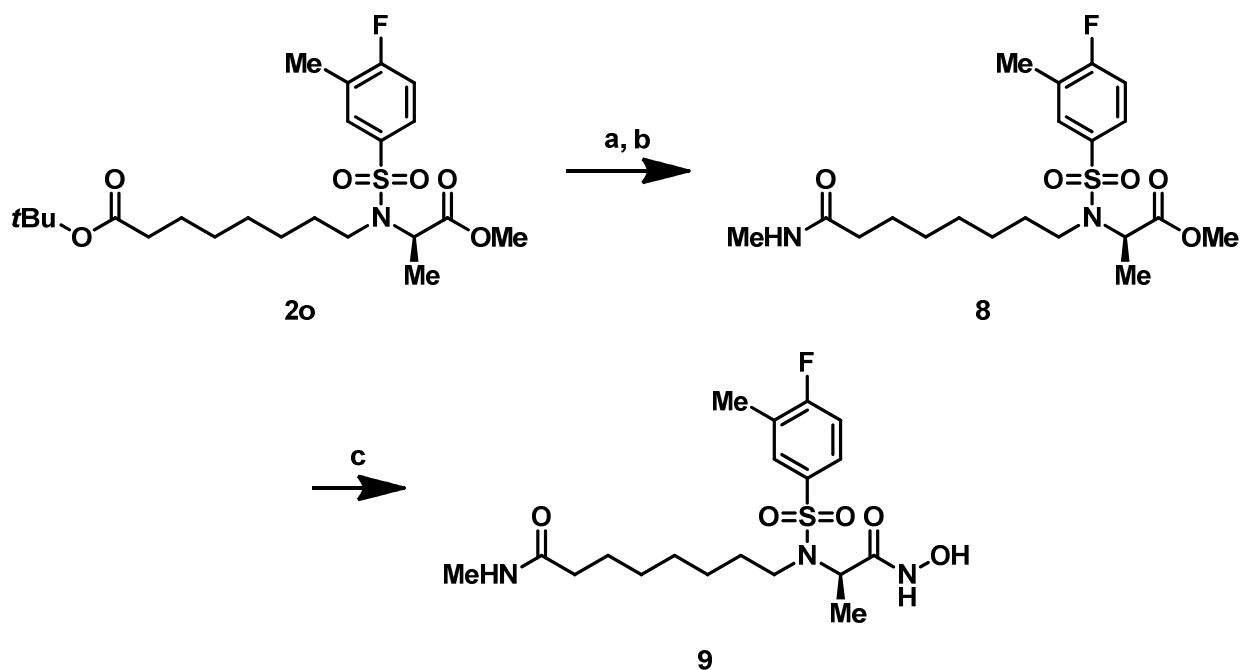
Reagents and Conditions: (a) 4 N HCl in dioxane, rt, 1 h; or TFA/DCM (1:2), TES, 0 °C.

Scheme 3. Synthesis of Compounds 7a-7f.



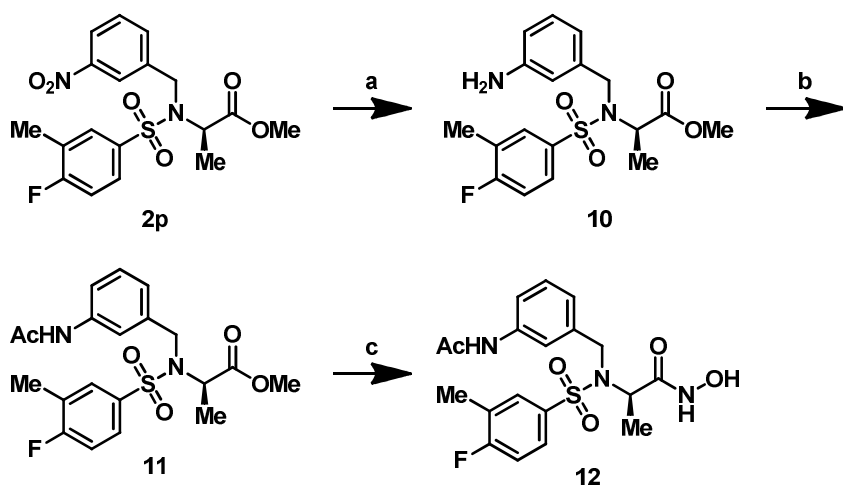
Reagents and Conditions: (a) 4 N HCl in dioxane, rt, 1 h; (b) Ac₂O, TEA, DMAP, THF, 0 °C, 16 h; (c) NH₂OH·HCl, NaOMe, MeOH, 0 °C to rt, 16 h.

Scheme 4. Synthesis of Compound 9.



Reagents and Conditions: (a) TFA/DCM (1:3), rt, 2.5 h; (b) $\text{CH}_3\text{NH}_2 \cdot \text{HCl}$, NMM, HOBt, EDC, THF, rt, 16 h; (c) $\text{NH}_2\text{OH} \cdot \text{HCl}$, NaOMe, MeOH, 0 °C to rt, 16 h.

Scheme 5. Synthesis of Compound 12.



Reagents and Conditions: (a) 10 wt. % Pd/C, MeOH, rt, 4h; (b) AcCl, TEA, DCM, 0 °C to rt, 16 h; (c) $\text{NH}_2\text{OH} \cdot \text{HCl}$, NaOMe, MeOH, 0 °C to rt, 16 h.

In vitro Assessment of LF inhibition

Two assays were used to measure the IC₅₀ values of the synthesized compounds: a quenched fluorescence resonance energy transfer (FRET) assay and a mobility shift assay (MSA). Details are provided below. The FRET assay measures LF enzymatic activity using an internally quenched peptide substrate derived from MAPKK. Briefly, LF cleavage separates the Dnp quencher from the oABz fluorescent tag, leading to an increase in fluorescence intensity. In order to address concerns about fluorescence interference, we employed a secondary, orthogonal MSA assay, which uses a microfluidic chip to measure the conversion of fluorescent substrate to fluorescent product. The terminated reaction mixture is introduced through a capillary sipper onto the chip, where substrate and product are separated by electrophoresis and detected via laser-induced fluorescence.

The MSA IC₅₀ values of all synthesized analogs ranged from 1.1 μM to 47 μM, which are consistently less favorable than the 0.5 μM IC₅₀ value demonstrated by the parent **3r** (Table 1). (Note that compounds **3b**, **3i**, **3k**, **3l**, **3m**, **3n**, and **3p** are not included in Table 1 because FRET and MSA triplicate data points unfortunately could not be obtained due to compound degradation).

DISCUSSION

From previously published crystallographic data⁵³ and the newer activity and structural data reported here, we can now ascertain that the S2' subsite of LF is able to accommodate many diverse N-alkylated analogs of **3r**. In our previous as well as in our more recent structures, the ligands align well and domain III is consistently observed to adopt the tight position. Interestingly, another analog (**3q**) that incorporates an isopropyl modification is inactive, likely

1
2
3 due to unavoidable steric clashes with Tyr728. Docking studies correctly predicted that **3q** would
4
5 prove to be the least active of the 28 synthesized compounds listed in Table 1. In subsequent
6
7 data, we observed that this steric clash with Tyr728 could be relieved by substituting the
8
9 isopropyl group with an *n*-propyl moiety, resulting in inhibitory activity of 6.4 μ M in the MSA.
10
11

12
13 The most active analogs from our new series incorporated primary amines into the N-
14
15 alkylated substituents. Our docking results shed further light on this, indicating that the improved
16
17 activity of primary amine-containing compounds may be due to additional interactions with the
18
19 $3\alpha 1$ - $3\alpha 2$ loop in domain III that separates the S2' subsite from the S4', specifically involving
20
21 electrostatic interactions with the Asp328 sidechain, and/or H-bond donating interactions with
22
23 the backbones of Asp325, Ser326 or Ser327. A notable exception is found in **5f**, which when
24
25 docked into both crystal structures, adopts a completely different orientation in the active site
26
27 and was not predicted to engage in interactions with any of those four residues. We note that
28
29 analog **5f** featured the shortest N-alkyl substituent (a three-carbon propyl linker), a moiety that is
30
31 likely too short to reach that particular set of residues.
32
33
34
35

36
37 Moreover, the amine-containing analogs **5a-5f** proved to be more active than their Boc-
38
39 protected or acetylated counterparts **3h**, **3j**, and **7a-7f**. Docking studies revealed that upon Boc-
40
41 protection or acetylation, analogs lose H-bond donating interactions with the backbone of
42
43 Asp325, Ser236, and Ser327, and also electrostatic interactions with Asp328. However,
44
45 carboxylic acid-containing compound **5g** exhibited a different pattern. The butyl protected
46
47 analog **3o** and the amide-containing analog **9** were both more active against LF than **5g**, which is
48
49 not surprising given that the carboxylic acid in **5g** is unable to donate a hydrogen bond to the
50
51 $3\alpha 1$ - $3\alpha 2$ loop. Also, hydrophobic compounds **3c-3g** do not engage in crucial protein-ligand
52
53
54
55
56
57
58
59
60

1
2
3 electrostatic or H-bond donating interactions with that loop, and are similarly less active than
4
5 amines **5a-5e**.
6
7
8
9

10 CONCLUSION

11
12 The S2' binding site of the anthrax toxin LF is a large, dynamic solvent exposed channel
13 that changes configuration in response to various ligands, such as our sulfonamide hydroxamate
14 **3r** analogs alkylated at the sulfonamide moiety, binding via the movement of domain III. We
15 synthesized a series of these analogs to take advantage of the residues that were exposed due to
16 this conformational change, and to probe binding preferences at this subsite. Biological activity
17 and X-ray data indicate that the decrease in inhibitory activity exhibited by these new analogs
18 with respect to the parent compound likely results from the elimination of a key ligand-receptor
19 H-bond to Tyr728. We did, however, find that biological activity can partly be recovered by
20 installing amine-containing substituents on the N-sulfonamide that are capable of interacting
21 with Asp325, Ser326 and Ser327. Possible steric clashes with Tyr728 decrease potency of
22 compounds dramatically; this should be taken into account during optimization of inhibitors with
23 groups that are oriented near this residue. Also, inhibitor design targeting the S2' subsite can
24 result in novel scaffolds with a wide variety of substituents that do not induce a significant loss
25 in potency, for example, 1.1 μM for **5c** compared to 0.5 μM for **3r**. One could therefore take
26 advantage of this accommodating S2' subsite to modify other scaffolds to improve druglike and
27 related properties.
28
29
30
31
32
33
34
35
36
37
38
39
40
41
42
43
44
45
46
47
48
49
50
51
52
53
54
55
56
57
58
59
60

EXPERIMENTAL SECTION

Biochemical Evaluation

Synthesized compounds were evaluated utilizing an *in vitro* fluorescence resonance energy transfer (FRET) and mobility shift (MSA) assays to determine LF inhibition as follows:

Quenched FRET Lethal Factor Protease Assay. The quenched fluorescence resonance energy transfer (FRET) assay measures LF enzymatic activity using an internally quenched peptide substrate derived from MAPKK. LF cleavage separates the Dnp quencher from the oABz fluorescent tag, leading to an increase in fluorescence intensity. Endpoint assays were conducted following modified published procedures.^{30,50} In this assay, 10 μ L of 100 nM anthrax toxin lethal factor prepared by us as described previously⁵¹ (final concentration 50 nM) in 2 X assay buffer (40 mM HEPES containing 0.02 % Triton X-100, pH 8.0) was added to 384-well assay plates (Corning #3677) using a MultiDrop (Thermo-Fisher). The plate was pre-incubated at 37 °C for 15 min and the reaction was initiated by the addition of 10 μ L of 14 μ M oAbz/Dnp-substrate (developed in-house at the Biomedical Genomics Center, University of Minnesota) in water (final substrate concentration 7 μ M). The reaction was allowed to continue for 5 minutes at 37 °C, and then terminated with addition of 5 μ L 50 mM EDTA (final concentration 10 mM). Fluorescence intensity was measured on a SpectraMax M2e microplate reader with excitation and emission wavelengths of 320 nm and 420 nm, respectively. For IC₅₀ determinations, test compounds were dissolved in DMSO at 10 mM and varying volumes were added to the assay plate using a Labcyte Echo® 550 acoustic dispenser prior to LF addition to achieve 8 concentrations in duplicate (final DMSO concentration 1 %). IC₅₀ values were determined as a percent of control wells containing no inhibitor (following subtraction of background wells lacking enzyme) from at least 3 independent experiments using GraphPad Prism software. IC₅₀

1
2
3 values were determined for the positive control compounds **13** and **14** (**GM6001**)³⁹ which were
4 included on every plate.
5
6

7
8 *Mobility Shift Protease Assay.* The off-chip mobility-shift assay uses a microfluidic chip
9 to measure the conversion of fluorescent substrate to fluorescent product using a Caliper LC3000
10 (PerkinElmer). The terminated reaction mixture is introduced through a capillary sipper onto the
11 chip where substrate and product are separated by electrophoresis and detected via laser-induced
12 fluorescence. As in the FRET assay, 10 μL of 100 nM anthrax toxin lethal factor prepared by us
13 as described previously⁵¹ (final concentration 50 nM) in 2X assay buffer (40 mM HEPES
14 containing 0.02 % Triton X-100, pH 8.0) was added to 384-well assay plates (Corning #3677)
15 using a MultiDrop (Thermo-Fisher). The plate was pre-incubated at 37 °C for 15 min and the
16 reaction was initiated by the addition of 10 μL of 8 μM FITC-substrate (Celtek Peptides, #RK-
17 10-4) in water (final substrate concentration 4 μM). The peptide sequence of the substrate is
18 identical to the FRET assay substrate. The reaction was allowed to continue for 10 minutes at 37
19 °C, and then terminated with addition of 4 μL 0.5 mM phenanthroline/32.5 μM EDTA solution
20 (final concentration of 0.1 mM phenanthroline /6.5 μM EDTA). Samples were then analyzed via
21 the LabChip 3000 software. For IC_{50} determinations, test compounds were dissolved in DMSO
22 at 10 mM and varying volumes were added to the assay plate using a Labcyte Echo® 550
23 acoustic dispenser prior to LF addition to achieve 8 concentrations in duplicate (final DMSO
24 concentration 1%). IC_{50} values were determined as a percent of control wells containing no
25 inhibitor (following subtraction of background wells lacking enzyme) from at least 3
26 independent experiments using GraphPad Prism software. As before, IC_{50} values were
27 determined for the positive control compounds **13** and **14** included on every plate.
28
29
30
31
32
33
34
35
36
37
38
39
40
41
42
43
44
45
46
47
48
49
50
51
52
53
54
55
56
57
58
59
60

1
2
3
4
5
6
7
8
9
10
11
12
13
14
15
16
17
18
19
20
21
22
23
24
25
26
27
28
29
30
31
32
33

Importantly, a high correlation between the quenched FRET and mobility shift assays was observed (see Supporting Information) indicating that both assays provide reliable inhibitory potency data for these compounds. On average, the compounds were 3.9-fold more potent in the mobility shift assay relative to the quenched FRET assay. This apparent potency difference is likely due to a 1.75-fold higher substrate concentration in the FRET relative to the mobility shift assay, and a higher substrate K_m in the mobility shift assay relative to that in the FRET assay. Although the amino acid sequence is identical in the substrates used in both assays, the N-terminal and C-terminal modifications are different, which may affect LF cleavage efficiency. Unfortunately, it is not technically feasible to determine the substrate K_m in the mobility shift assay because signal linearity is lost at high concentrations of substrate. The higher substrate concentration in the FRET assay coupled with a higher K_m in the mobility shift assay would decrease the apparent potency of these competitive inhibitors in the FRET assay.

34 35 36 37 38 39 40 41 42 43 44 45 46 47 48 49 50 51 52 53 54 55 56 57 58 59 60

Structural Biology

Lethal factor protein (residues 265-776, A266S) was prepared and small molecule ligands were co-crystallized as reported by us.⁵³ Diffraction data for structure 4WF6 (**3r**) were collected at 100 K using a Saturn 944+ detector and a Rigaku Miromax-007FHM source in-house (at the University of Minnesota). The data were processed using HKL2000.⁶² Diffraction data for structures 5D1S (**3a**), 5D1T (**5a**), and 5D1U (**5c**) were collected at 100 K on beamline 17-ID-B (IMCA-CAT) using a Dectris PILATUS 6M pixel-array detector at the Advanced Photon Source, at Argonne National Laboratories in Argonne, IL. The data were processed using autoPROC.⁶³ The structures were solved using molecular replacement with atomic coordinates from either 1YQY or 4PKR using Phaser⁶⁴ in the CCP4 suite.⁶⁵ Structural refinement was done

1
2
3 using both Refmac⁵⁶⁶ and Phenix,^{67,68} while the Coot modeling software⁶⁹ was used for
4
5
6 visualization and model building. Ligand omit maps are provided in Supporting Information.
7
8
9

10 **ANCILLARY INFORMATION**

11 **Supporting Information**

12
13
14
15 Details of chemical synthesis, compound characterization data, docking and scoring
16
17 algorithm selection, X-ray crystal structure selection for docking and scoring, correlation data
18
19 between the quenched FRET and mobility shift assays, X-ray crystallographic omit maps, and a
20
21 table of SMILES strings (in CSV format) and IC₅₀ values for each compound reported here.
22
23

24 **Accession Codes**

25
26
27 Coordinates of 4WF6, 5D1S, 5D1T, and 5D1U have been deposited in the Protein Data
28
29 Bank.
30
31

32 **Corresponding Author**

33
34
35 Elizabeth Ambrose Amin; E-mail: eamin@umn.edu. Telephone: 612-626-2387. Fax: 612-626-
36
37 6346
38
39

40 **Notes**

41
42 The authors declare no competing financial interest.
43
44

45 **Acknowledgments**

46
47 This work was funded partly by NIH/NIAID R01 AI083234, the University of Minnesota
48
49 Office of the Vice President for Research (Grant-in-Aid of Research, Artistry, and Scholarship),
50
51 and the University of Minnesota College of Pharmacy Grants Award Program, all to E.A.A.
52
53
54 Additional support was provided by the University of Minnesota Doctoral Dissertation
55
56 Fellowship, and the University of Minnesota College of Pharmacy Bighley Fellowship, both
57
58
59
60

1
2
3 awarded to E.K.K., and the American Foundation for Pharmaceutical Education Pre-Doctoral
4
5 Fellowship, awarded to K.M.M. The authors gratefully acknowledge the Minnesota
6
7 Supercomputing Institute for Advanced Computational Research (MSI), particularly Ms. Nancy
8
9 Rowe, for valuable assistance. The authors would also like to thank Teresa de la Mora-Rey for
10
11 initial structural work. Use of the IMCA-CAT beamline 17-ID at the Advanced Photon Source
12
13 was supported by the companies of the Industrial Macromolecular Crystallography Association
14
15 through a contract with Hauptman-Woodward Medical Research Institute.
16
17
18

19 **Abbreviations Used**

20
21 LF, Anthrax Toxin Lethal Factor; CDC, Centers for Disease Control; FDA, Food and Drug
22
23 Administration; EF, Anthrax Toxin Edema Factor; PA, Anthrax Toxin Protective Antigen;
24
25 MAPKKs, mitogen-activated protein kinase kinases; SNS, Strategic National Stockpile; NHPs,
26
27 non-human primates; NZW, New Zealand white; MMPs, matrix metalloproteinases; ZBGs, zinc-
28
29 binding groups; MSA, mobility shift assay; Dnp, 2,4-dinitrophenyl; o-Abz, o-aminobenzoic acid.
30
31
32
33
34
35
36
37
38
39
40
41
42
43
44
45
46
47
48
49
50
51
52
53
54
55
56
57
58
59
60

REFERENCES

- (1) Famous Cases and Criminals. <https://www.fbi.gov/about-us/history/famous-cases/anthrax-amerithrax> (accessed Jul 23, 2015).
- (2) Anthrax. <http://www.cdc.gov/anthrax/bioterrorism/threat.html> (accessed Jul 23, 2015).
- (3) Inglesby, T. V.; O'Toole, T.; Henderson, D. A.; Bartlett, J. G.; Ascher, M. S.; Eitzen, E.; Friedlander, A. M.; Gerberding, J.; Hauer, J.; Hughes, J.; McDade, J.; Osterholm, M. T.; Parker, G.; Perl, T. M.; Russell, P. K.; Tonat, K. Anthrax as a Biological Weapon, 2002: Updated Recommendations for Management. *JAMA* **2002**, *287*, 2236–2252.
- (4) Riedel, S. Anthrax: A Continuing Concern in the Era of Bioterrorism. *Proc. Bayl. Univ. Med. Cent.* **2005**, *18*, 234–243.
- (5) Meselson, M.; Guillemin, J.; Hugh-Jones, M.; Langmuir, A.; Popova, I.; Shelokov, A.; Yampolskaya, O. The Sverdlovsk Anthrax Outbreak of 1979. *Science* **1994**, *266*, 1202–1208.
- (6) Pezard, C.; Berche, P.; Mock, M. Contribution of Individual Toxin Components to Virulence of Bacillus Anthracis. *Infect. Immun.* **1991**, *59*, 3472–3477.
- (7) Chopra, P. A.; Boone, A. S.; Liang, X.; Duesbery, S. N.; Anthrax Lethal Factor Proteolysis and Inactivation of MAPK Kinase. *J. Biol. Chem.* **2003**, *278*, 9402–9406.
- (8) Vitale, G.; Bernardi, L.; Napolitani, G.; Mock, M.; Montecucco, C. Susceptibility of Mitogen-Activated Protein Kinase Kinase Family Members to Proteolysis by Anthrax Lethal Factor. *Biochem. J.* **2000**, *352*, 739–745.
- (9) Biondi, R. M.; Nebreda, A. R. Signalling Specificity of Ser/Thr Protein Kinases through Docking-Site-Mediated Interactions. *Biochem. J.* **2003**, *372*, 1–13.
- (10) Tanoue, T.; Nishida, E. Molecular Recognitions in the MAP Kinase Cascades. *Cell. Signalling* **2003**, *15*, 455–462.

- 1
2
3
4
5
6
7
8
9
10
11
12
13
14
15
16
17
18
19
20
21
22
23
24
25
26
27
28
29
30
31
32
33
34
35
36
37
38
39
40
41
42
43
44
45
46
47
48
49
50
51
52
53
54
55
56
57
58
59
60
- (11) Bardwell, A. J.; Abdollahi, M.; Bardwell, L. Anthrax Lethal Factor-Cleavage Products of MAPK (mitogen-Activated Protein Kinase) Kinases Exhibit Reduced Binding to Their Cognate MAPKs. *Biochem. J.* **2004**, *378*, 569–577.
- (12) Duesbery, N. S.; Webb, C. P.; Leppla, S. H.; Gordon, V. M.; Klimpel, K. R.; Copeland, T. D.; Ahn, N. G.; Oskarsson, M. K.; Fukasawa, K.; Paull, K. D.; Vande Woude, G. F. Proteolytic Inactivation of MAP-Kinase-Kinase by Anthrax Lethal Factor. *Science* **1998**, *280*, 734–737.
- (13) Moayeri, M.; Leppla, S. H. The Roles of Anthrax Toxin in Pathogenesis. *Curr. Opin. Microbiol.* **2004**, *7*, 19-24.
- (14) Warfel, J. M.; Steele, A. D.; D’Agnillo, F. Anthrax Lethal Toxin Induces Endothelial Barrier Dysfunction. *Am. J. Pathol.* **2005**, *166*, 1871–1881.
- (15) Liu, T.; Milia, E.; Warburton, R. R.; Hill, N. S.; Gaestel, M.; Kayyali, U. S. Anthrax Lethal Toxin Disrupts the Endothelial Permeability Barrier through Blocking p38 Signaling. *J. Cell. Physiol.* **2012**, *227*, 1438–1445.
- (16) Dixon, T. C.; Meselson, M.; Guillemin, J.; Hanna, P. C. Anthrax. *N. Engl. J. Med.* **1999**, *341*, 815–826.
- (17) Chames, P.; Van Regenmortel, M.; Weiss, E.; Baty, D. Therapeutic Antibodies: Successes, Limitations and Hopes for the Future. *Br. J. Pharmacol.* **2009**, *157*, 220–233.
- (18) Carter, P. J. Potent Antibody Therapeutics by Design. *Nat. Rev. Immunol.* **2006**, *6*, 343–357.
- (19) Valortim. <http://www.pharmathene.com/product-portfolio/valortim-anthrax-anti-toxin> (accessed Aug 13, 2015).

- 1
2
3 (20) Migone, T.-S.; Subramanian, G. M.; Zhong, J.; Healey, L. M.; Corey, A.; Devalaraja, M.;
4
5 Lo, L.; Ullrich, S.; Zimmerman, J.; Chen, A.; Lewis, M.; Meister, G.; Gillum, K.; Sanford, D.;
6
7 Mott, J.; Bolmer, S. D. Raxibacumab for the Treatment of Inhalational Anthrax. *N. Engl. J. Med.*
8
9 **2009**, *361*, 135–144.
- 10
11
12 (21) Corey, A.; Migone, T.-S.; Bolmer, S.; Fiscella, M.; Ward, C.; Chen, C.; Meister, G.
13
14 Bacillus Anthracis Protective Antigen Kinetics in Inhalation Spore-Challenged Untreated or
15
16 Levofloxacin/ Raxibacumab-Treated New Zealand White Rabbits. *Toxins* **2013**, *5*, 120–138.
- 17
18
19 (22) Anthrasil [package Insert]. Winnipeg, Canada: Cangene Corporation; 2015.
- 20
21
22 (23) Sellman, B. R.; Mourez, M.; Collier, R. J. Dominant-Negative Mutants of a Toxin
23
24 Subunit: An Approach to Therapy of Anthrax. *Science* **2001**, *292*, 695–697.
- 25
26
27 (24) Min, D.-H.; Tang, W.-J.; Mrksich, M. Chemical Screening by Mass Spectrometry to
28
29 Identify Inhibitors of Anthrax Lethal Factor. *Nat. Biotechnol.* **2004**, *22*, 717–723.
- 30
31
32 (25) Pannifer, A. D.; Wong, T. Y.; Schwarzenbacher, R.; Renatus, M.; Petosa, C.;
33
34 Bienkowska, J.; Lacy, D. B.; Collier, R. J.; Park, S.; Leppla, S. H.; Hanna, P.; Liddington, R. C.
35
36 Crystal Structure of the Anthrax Lethal Factor. *Nature* **2001**, *414*, 229–233.
- 37
38
39 (26) Whittaker, M.; Floyd, C. D.; Brown, P.; Gearing, A. J. Design and Therapeutic
40
41 Application of Matrix Metalloproteinase Inhibitors. *Chem. Rev.* **1999**, *99*, 2735–2776.
- 42
43
44 (27) Xiong, Y.; Wiltsie, J.; Woods, A.; Guo, J.; Pivnichny, J. V.; Tang, W.; Bansal, A.;
45
46 Cummings, R. T.; Cunningham, B. R.; Friedlander, A. M.; Douglas, C. M.; Salowe, S. P.; Zaller,
47
48 D. M.; Scolnick, E. M.; Schmatz, D. M.; Bartizal, K.; Hermes, J. D.; MacCoss, M.; Chapman, K.
49
50 T. The Discovery of a Potent and Selective Lethal Factor Inhibitor for Adjunct Therapy of
51
52 Anthrax Infection. *Bioorg. Med. Chem. Lett.* **2006**, *16*, 964–968.
- 53
54
55
56
57
58
59
60

- 1
2
3
4
5
6
7
8
9
10
11
12
13
14
15
16
17
18
19
20
21
22
23
24
25
26
27
28
29
30
31
32
33
34
35
36
37
38
39
40
41
42
43
44
45
46
47
48
49
50
51
52
53
54
55
56
57
58
59
60
- (28) Forino, M.; Johnson, S.; Wong, T. Y.; Rozanov, D. V.; Savinov, A. Y.; Li, W.; Fattorusso, R.; Becattini, B.; Orry, A. J.; Jung, D.; Abagyan, R. A.; Smith, J. W.; Alibek, K.; Liddington, R. C.; Strongin, A. Y.; Pellecchia, M. Efficient Synthetic Inhibitors of Anthrax Lethal Factor. *Proc. Natl. Acad. Sci. U. S. A.* **2005**, *102*, 9499–9504.
- (29) Johnson, S. L.; Jung, D.; Forino, M.; Chen, Y.; Satterthwait, A.; Rozanov, D. V.; Strongin, A. Y.; Pellecchia, M. Anthrax Lethal Factor Protease Inhibitors: Synthesis, SAR, and Structure-Based 3D QSAR Studies. *J. Med. Chem.* **2006**, *49*, 27-30.
- (30) Goldman, E.; Cregar, L.; Nguyen, D.; Simo, O.; O'Malley, S.; Humphreys, T. Cationic Polyamines Inhibit Anthrax Lethal Factor Protease. *BMC Pharmacol.* **2006**, *6*, 1–8.
- (31) Schepetkin, I. A.; Khlebnikov, A. I.; Kirpotina, L. N.; Quinn, M. T. Novel Small-Molecule Inhibitors of Anthrax Lethal Factor Identified by High-Throughput Screening. *J. Med. Chem.* **2006**, *49*, 5232–5244.
- (32) Karginov, V. A.; Nestorovich, E. M.; Moayeri, M.; Leppla, S. H.; Bezrukov, S. M. Blocking Anthrax Lethal Toxin at the Protective Antigen Channel by Using Structure-Inspired Drug Design. *Proc. Natl. Acad. Sci. U. S. A.* **2005**, *102*, 15075–15080.
- (33) Jiao, G.-S.; Kim, S.; Moayeri, M.; Crown, D.; Thai, A.; Cregar-Hernandez, L.; McKasson, L.; Sankaran, B.; Lehrer, A.; Wong, T.; Johns, L.; Margosiak, S. A.; Leppla, S. H.; Johnson, A. T. Antidotes to Anthrax Lethal Factor Intoxication. Part 3: Evaluation of Core Structures and Further Modifications to the C2-Side Chain. *Bioorg. Med. Chem. Lett.* **2012**, *22*, 2242–2246.
- (34) Dalkas, G. A.; Papakyriakou, A.; Vlamis-Gardikas, A.; Spyroulias, G. A. Low Molecular Weight Inhibitors of the Protease Anthrax Lethal Factor. *Mini Rev. Med. Chem.* **2008**, *8*, 290-306.

- 1
2
3
4 (35) Verma, R. P.; Hansch, C. Combating the Threat of Anthrax: A Quantitative Structure-
5 Activity Relationship Approach. *Mol. Pharm.* **2008**, *5*, 745–759.
6
7
8 (36) Gaddis, B. D.; Avramova, L. V.; Chmielewski, J. Inhibitors of Anthrax Lethal Factor.
9
10 *Bioorg. Med. Chem. Lett.* **2007**, *17*, 4575–4578.
11
12
13 (37) Turk, B. E. Discovery and Development of Anthrax Lethal Factor Metalloproteinase
14 Inhibitors. *Curr. Pharm. Biotechnol.* **2008**, *9*, 24-33.
15
16
17 (38) Tonello, F.; Seveso, M.; Marin, O.; Mock, M.; Montecucco, C. Pharmacology: Screening
18 Inhibitors of Anthrax Lethal Factor. *Nature* **2002**, *418*, 386–386.
19
20
21
22 (39) Turk, B. E.; Wong, T. Y.; Schwarzenbacher, R.; Jarrell, E. T.; Leppla, S. H.; Collier, R.
23 J.; Liddington, R. C.; Cantley, L. C. The Structural Basis for Substrate and Inhibitor Selectivity
24 of the Anthrax Lethal Factor. *Nat. Struct. Mol. Biol.* **2004**, *11*, 60–66.
25
26
27
28
29 (40) Panchal, R. G.; Hermone, A. R.; Nguyen, T. L.; Wong, T. Y.; Schwarzenbacher, R.;
30 Schmidt, J.; Lane, D.; McGrath, C.; Turk, B. E.; Burnett, J.; Aman, M. J.; Little, S.; Sausville, E.
31 A.; Zaharevitz, D. W.; Cantley, L. C.; Liddington, R. C.; Gussio, R.; Bavari, S. Identification of
32 Small Molecule Inhibitors of Anthrax Lethal Factor. *Nat. Struct. Mol. Biol.* **2004**, *11*, 67-72.
33
34
35
36
37
38 (41) Lee, L. V.; Bower, K. E.; Liang, F.-S.; Shi, J.; Wu, D.; Sucheck, S. J.; Vogt, P. K.; Wong,
39 C.-H. Inhibition of the Proteolytic Activity of Anthrax Lethal Factor by Aminoglycosides. *J. Am.*
40 *Chem. Soc.* **2004**, *126*, 4774–4775.
41
42
43
44
45
46 (42) Kocer, S. S.; Walker, S. G.; Zerler, B.; Golub, L. M.; Simon, S. R. Metalloproteinase
47 Inhibitors, Nonantimicrobial Chemically Modified Tetracyclines, and Ilomastat Block Bacillus
48 Anthracis Lethal Factor Activity in Viable Cells. *Infect. Immun.* **2005**, *73*, 7548–7557.
49
50
51
52
53
54
55
56
57
58
59
60

- 1
2
3
4
5
6
7
8
9
10
11
12
13
14
15
16
17
18
19
20
21
22
23
24
25
26
27
28
29
30
31
32
33
34
35
36
37
38
39
40
41
42
43
44
45
46
47
48
49
50
51
52
53
54
55
56
57
58
59
60
- (43) Johnson, S. L.; Chen, L.-H.; Harbach, R.; Sabet, M.; Savinov, A.; Cotton, N. J. H.; Strongin, A.; Guiney, D.; Pellicchia, M. Rhodanine Derivatives as Selective Protease Inhibitors against Bacterial Toxins. *Chem. Biol. Drug Des.* **2008**, *71*, 131–139.
- (44) Houseman, B. T.; Huh, J. H.; Kron, S. J.; Mrksich, M. Peptide Chips for the Quantitative Evaluation of Protein Kinase Activity. *Nat. Biotechnol.* **2002**, *20*, 270–274.
- (45) Min, D.-H.; Su, J.; Mrksich, M. Profiling Kinase Activities by Using a Peptide Chip and Mass Spectrometry. *Angew. Chem. Int. Ed.* **2004**, *43*, 5973–5977.
- (46) Su, J.; Mrksich, M. Using Mass Spectrometry to Characterize Self-Assembled Monolayers Presenting Peptides, Proteins, and Carbohydrates. *Angew. Chem. Int. Ed.* **2002**, *41*, 4715–4718.
- (47) Dell’Aica, I. D.; Tonello, M.; Piris, F.; Mock, A.; Montecucco, M.; Garbisa, C.; Spiridione. Potent Inhibitors of Anthrax Lethal Factor from Green Tea. *EMBO Rep.* **2004**, *5*, 418–422.
- (48) Kim, C.; Gajendran, N.; Mittrucker, H.-W.; Weiwad, M.; Song, Y.-H.; Hurwitz, R.; Wilmanns, M.; Fischer, G.; Kaufmann, S. H. E. Human Alpha-Defensins Neutralize Anthrax Lethal Toxin and Protect against Its Fatal Consequences. *Proc. Natl. Acad. Sci. U. S. A.* **2005**, *102*, 4830–4835.
- (49) Johnson, S. L.; Chen, L.-H.; Pellicchia, M. A High-Throughput Screening Approach to Anthrax Lethal Factor Inhibition. *Bioorganic Chem.* **2007**, *35*, 306–312.
- (50) Shoop, W. L.; Xiong, Y.; Wiltsie, J.; Woods, A.; Guo, J.; Pivnichny, J. V.; Felcetto, T.; Michael, B. F.; Bansal, A.; Cummings, R. T.; Cunningham, B. R.; Friedlander, A. M.; Douglas, C. M.; Patel, S. B.; Wisniewski, D.; Scapin, G.; Salowe, S. P.; Zaller, D. M.; Chapman, K. T.;

1
2
3 Scolnick, E. M.; Schmatz, D. M.; Bartizal, K.; MacCoss, M.; Hermes, J. D. Anthrax Lethal
4 Factor Inhibition. *Proc. Natl. Acad. Sci. U. S. A.* **2005**, *102*, 7958–7963.

5
6
7
8 (51) Chiu, T.-L.; Solberg, J.; Patil, S.; Geders, T. W.; Zhang, X.; Rangarajan, S.; Francis, R.;
9 Finzel, B. C.; Walters, M. A.; Hook, D. J.; Amin, E. A. Identification of Novel Non-
10 Hydroxamate Anthrax Toxin Lethal Factor Inhibitors by Topomeric Searching, Docking and
11 Scoring, and in Vitro Screening. *J. Chem. Inf. Model.* **2009**, *49*, 2726–2734.

12
13
14
15 (52) Chiu, T.-L.; Amin, E. A. Development of a Comprehensive, Validated Pharmacophore
16 Hypothesis for Anthrax Toxin Lethal Factor (LF) Inhibitors Using Genetic Algorithms, Pareto
17 Scoring, and Structural Biology. *J. Chem. Inf. Model.* **2012**, *52*, 1886–1897.

18
19
20
21
22 (53) Maize, K. M.; Kurbanov, E. K.; De La Mora-Rey, T.; Geders, T. W.; Hwang, D.-J.;
23 Walters, M. A.; Johnson, R. L.; Amin, E. A.; Finzel, B. C. Anthrax Toxin Lethal Factor Domain
24 3 Is Highly Mobile and Responsive to Ligand Binding. *Acta Crystallogr. Sect. D: Biol.*
25 *Crystallogr.* **2014**, *70*, 2813–2822.

26
27
28 (54) Glide, Version 5.9, Schrödinger, LLC, New York, NY, 2014.

29
30
31
32 (55) Friesner, R. A.; Banks, J. L.; Murphy, R. B.; Halgren, T. A.; Klicic, J. J.; Mainz, D. T.;
33 Repasky, M. P.; Knoll, E. H.; Shelley, M.; Perry, J. K.; Shaw, D. E.; Francis, P.; Shenkin, P. S.
34 Glide: A New Approach for Rapid, Accurate Docking and Scoring. 1. Method and Assessment
35 of Docking Accuracy. *J. Med. Chem.* **2004**, *47*, 1739–1749.

36
37
38
39 (56) Friesner, R. A.; Murphy, R. B.; Repasky, M. P.; Frye, L. L.; Greenwood, J. R.; Halgren,
40 T. A.; Sanschagrin, P. C.; Mainz, D. T. Extra Precision Glide: Docking and Scoring
41 Incorporating a Model of Hydrophobic Enclosure for Protein-Ligand Complexes. *J. Med. Chem.*
42 **2006**, *49*, 6177–6196.

- 1
2
3
4
5
6
7
8
9
10
11
12
13
14
15
16
17
18
19
20
21
22
23
24
25
26
27
28
29
30
31
32
33
34
35
36
37
38
39
40
41
42
43
44
45
46
47
48
49
50
51
52
53
54
55
56
57
58
59
60
- (57) Halgren, T. A.; Murphy, R. B.; Friesner, R. A.; Beard, H. S.; Frye, L. L.; Pollard, W. T.; Banks, J. L. Glide: A New Approach for Rapid, Accurate Docking and Scoring. 2. Enrichment Factors in Database Screening. *J. Med. Chem.* **2004**, *47*, 1750–1759.
- (58) Jain, A. N. Surflex-Dock 2.1: Robust Performance from Ligand Energetic Modeling, Ring Flexibility, and Knowledge-Based Search. *J. Comput. Aided Mol. Des.* **2007**, *21*, 281-306.
- (59) Jain, A. N. Surflex: Fully Automatic Flexible Molecular Docking Using a Molecular Similarity-Based Search Engine. *J. Med. Chem.* **2003**, *46*, 499-511.
- (60) Morris, G. M.; Huey, R.; Lindstrom, W.; Sanner, M. F.; Belew, R. K.;Goodsell, D. S.; Olson, A. J. AutoDock4 and AutoDockTools4: Automated Docking with Selective Receptor Flexibility. *J. Comput. Chem.* **2009**, *30*, 2785–2791.
- (61) Molecular Operating Environment (MOE), 2013.08; Chemical Computing Group Inc., 1010 Sherbooke St. West, Suite #910, Montreal, QC, Canada, H3A 2R7, 2015.
- (62) Otwinowski, Z; Minor, W. Processing of X-ray Diffraction Data Collected in Oscillation Mode. In *Methods in Enzymology*, C. W. Carter, Jr., C. W., Sweet, R. M., Eds.; Academic Press: New York, 1997; Vol. 276, Macromolecular Crystallography, part A, pp 307-326.
- (63) Evans, P. Scaling and Assessment of Data Quality. *Acta Crystallogr. Sect. D: Biol. Crystallogr.* **2006**, *62*, 72–82.
- (64) McCoy, A. J.; Grosse-Kunstleve, R. W.; Adams, P. D.; Winn, M. D.; Storoni, L. C.; Read, R. J. Phaser Crystallographic Software. *J. Appl. Crystallogr.* **2007**, *40*, 658–674.
- (65) Winn, M. D.; Ballard, C. C.; Cowtan, K. D.; Dodson, E. J.; Emsley, P.; Evans, P. R.; Keegan, R. M.; Krissinel, E. B.; Leslie, A. G. W.; McCoy, A.; McNicholas, S. J.; Murshudov, G. N.; Pannu, N. S.; Potterton, E. A.; Powell, H. R.; Read, R. J.; Vagin, A.; Wilson, K. S. Overview

1
2
3 of the CCP4 Suite and Current Developments. *Acta Crystallogr. Sect. D: Biol. Crystallogr.* **2011**,
4
5
6 67, 235–242.

7
8 (66) Murshudov, G. N.; Skubak, P.; Lebedev, A. A.; Pannu, N. S.; Steiner, R. A.; Nicholls, R.
9
10 A.; Winn, M. D.; Long, F.; Vagin, A. A. REFMAC5 for the Refinement of Macromolecular
11
12 Crystal Structures. *Acta Crystallogr. Sect. D: Biol. Crystallogr.* **2011**, 67, 355–367.

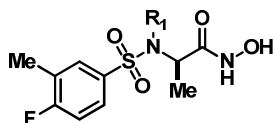
13
14
15 (67) Adams, P. D.; Afonine, P. V.; Bunkoczi, G.; Chen, V. B.; Davis, I. W.; Echols, N.;
16
17 Headd, J. J.; Hung, L.-W.; Kapral, G. J.; Grosse-Kunstleve, R. W.; McCoy, A. J.; Moriarty, N.
18
19 W.; Oeffner, R.; Read, R. J.; Richardson, D. C.; Richardson, J. S.; Terwilliger, T. C.; Zwart, P.
20
21 H. PHENIX: A Comprehensive Python-Based System for Macromolecular Structure Solution.
22
23
24 *Acta Crystallogr. Sect. D: Biol. Crystallogr.* **2010**, 66, 213–221.

25
26
27 (68) Afonine, P. V.; Grosse-Kunstleve, R. W.; Echols, N.; Headd, J. J.; Moriarty, N. W.;
28
29 Mustyakimov, M.; Terwilliger, T. C.; Urzhumtsev, A.; Zwart, P. H.; Adams, P. D. Towards
30
31 Automated Crystallographic Structure Refinement with Phenix.refine. *Acta Crystallogr. Sect. D:*
32
33
34 *Biol. Crystallogr.* **2012**, 68, 352–367.

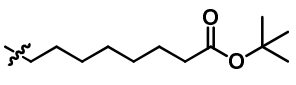
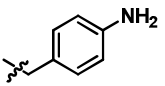
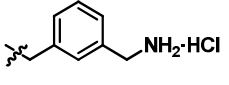
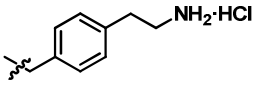
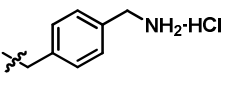
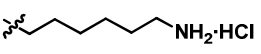
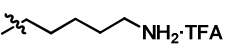
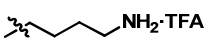
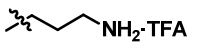
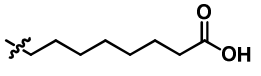
35
36
37 (69) Emsley, P.; Cowtan, K. Coot: Model-Building Tools for Molecular Graphics. *Acta*
38
39
40
41
42
43
44
45
46
47
48
49
50
51
52
53
54
55
56
57
58
59
60
Crystallogr. Sect. D: Biol. Crystallogr. **2004**, 60, 2126–2132.

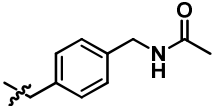
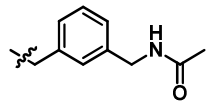
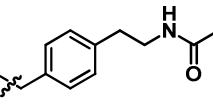
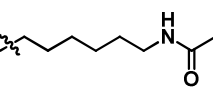
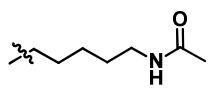
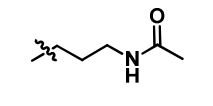
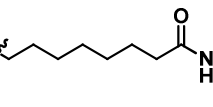
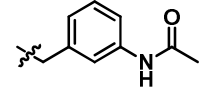
Tables

Table 1. Novel series of **3r**-based LF inhibitors bearing various substitutions at R₁, with corresponding LF biological activity values from FRET and MSA assays. Compounds **3b**, **3i**, **3k**, **3l**, **3m**, **3n**, and **3p** are not included here because FRET and MSA triplicate data points could not be obtained due to compound degradation.



Compound	R ¹	MSA ^b	FRET
		IC ₅₀ (μM) ^c	IC ₅₀ (μM) ^c
3a	Me	9.6 ± 0.1	37 ± 5
3c		7.0 ± 2	26 ± 5
3d		11 ± 3	29 ± 5
3e		9.5 ± 2	33 ± 3
3f		13 ± 2	42 ± 1
3g		14 ± 0.6	57 ± 6
3h		3.4 ± 0.1	15 ± 0.9
3j		2.1 ± 0.1	6.9 ± 1

3o		3.2 ± 0.3	8.0 ± 0.9
3q	isopropyl	>100	>100
3r	H	0.5 ± 0.1	1.6 ± 0.1
4a		6.4 ± 0.7	29 ± 6
5a		1.7 ± 0.1	10 ± 2
5b		1.2 ± 0.1	8.9 ± 0.6
16*		1.3 ± 0.1	5.6 ± 0.3
5c		1.1 ± 0.1	4.4 ± 0.2
5d		1.3 ± 0.2	8.2 ± 0.3
5e		1.8 ± 0.1	7.4 ± 0.6
5f		3.7 ± 0.8	12 ± 3
5g		47 ± 2	91 ± 4

7a		3.5 ± 0.3	16 ± 4
7b		4.7 ± 0.5	15 ± 2
7c		3.2 ± 0.3	17 ± 2
7d		3.9 ± 0.5	14 ± 1
7e		4.3 ± 0.5	19 ± 3
7f		30 ± 2	117 ± 18
9		9.3 ± 1	19 ± 3
12		4.8 ± 0.2	21 ± 2

^aMSA = mobility shift assay

^bIC₅₀ is reported as the mean of 3 independent assay results

*reported previously⁵³

Figures

Figure 1: Anthrax toxin LF inhibitor binding groove at the interface of LF domains 2 (wheat), 3 (cyan) and 4 (white), and peptide-binding subsites as revealed by the complex with peptide substrates (PDB ID 1PWW)³⁹. (a) Alkylations at the sulfonamide nitrogen of **13** (green) should vector toward the S2' proline in peptide substrates. The peptide from PDB structure 1PWW is shown (teal). (b) Known inhibitors poorly sample the chemical moiety preferences in the S2' subsite. Structures shown include 1PWP⁴⁰ (yellow), 1PWQ³⁹ (cyan), 1PWU³⁹ (**14**; magenta), 1ZXV²⁸ (salmon), 4DV8³³ (blue), and 1YQY⁵⁰ (**13**, green). Only one of these (**14**) occupies any depth of the S2'.

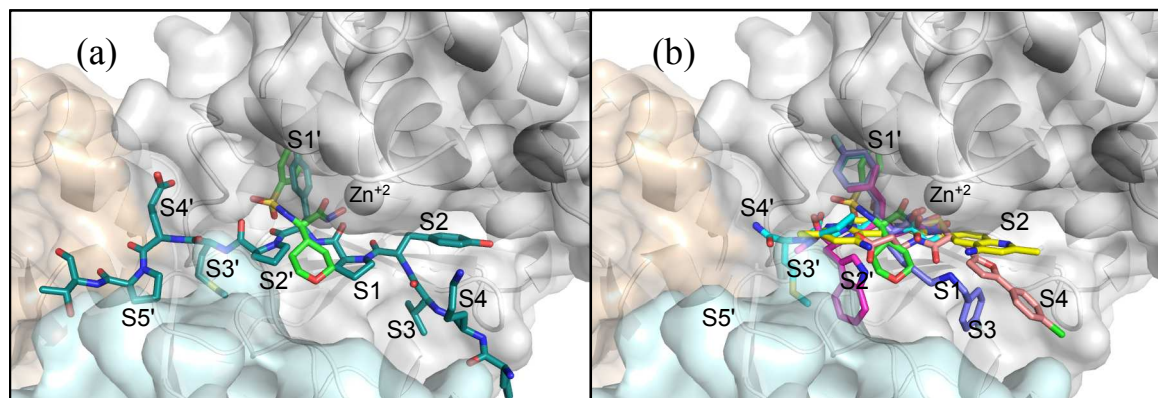
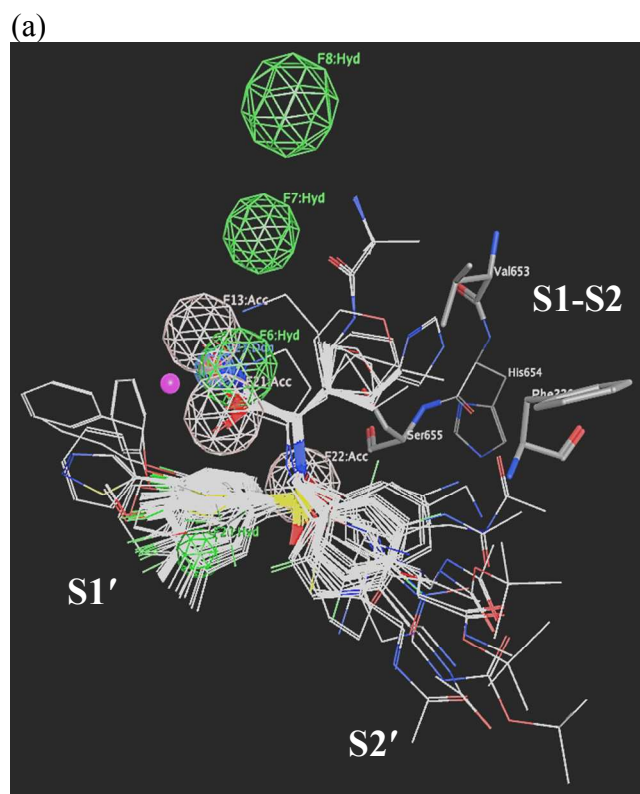


Figure 2: (a) Previously published comprehensive LF pharmacophore hypothesis **UM1** for LF inhibitors,⁵² shown with the training set compounds implemented in the current CoMSIA study, catalytic Zn^{2+} (magenta sphere), and three binding subsites displayed (MOE 2010.10). Three residues playing key roles in ligand binding (Val 653, Ser 655, Phe329) in the S1-S2 subsite are illustrated in stick format. (b) List of features and their radii in **UM1**: Hyd = hydrophobic; Acc = hydrogen-bond acceptor; Don = hydrogen-bond donor. Blue sphere: hydrogen-bond donor feature F23 at the hydroxamate NH.



(b)

Feature ID	Feature Type	Radius (Å)	Interacting residues in the LF active site
F6	Hyd	1.3	residues in the hydrophobic S1-S2 and zinc-chelating regions of the LF active site
F7	Hyd	1.2	
F8	Hyd	1.5	
F13	Acc	1.3	Glu687 near the catalytic Zn^{2+}
F20	Hyd	0.8	zinc-binding residue His686, Tyr728 in the S1-S2 subsite, Leu677 in the S1' subsite, and Lys656 at the S2' entrance
F21	Acc	1.3	Glu735 and Tyr728 in the S1-S2 subsite
F22	Acc	1.3	Gly657 near the bottom of the active site and Lys656 at the S2' entrance
F23	Don	0.7	Gly657 near the bottom of the active site and Glu687 near the catalytic Zn^{2+}

1
2
3
4
5
6
7
8
9
10
11
12
13
14
15
16
17
18
19
20
21
22
23
24
25
26
27
28
29
30
31
32
33
34
35
36
37
38
39
40
41
42
43
44
45
46
47
48
49
50
51
52
53
54
55
56
57
58
59
60

Figure 3. Sulfonamide hydroxamate LF inhibitors: a) **13**; b) **14**

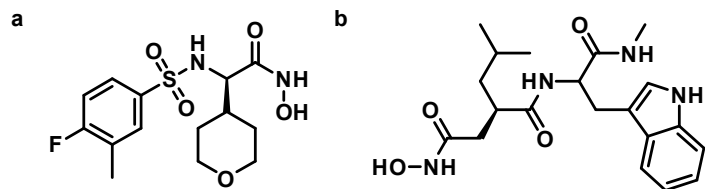


Figure 4. Experimental X-ray binding modes of (a) **13** (tan, PDB ID 1YQY) and **3r** (green, PDB ID 4WF6), illustrating that these compounds bind to LF in similar modes and engage in the same hydrogen bonds; and (b) compounds **3r** (green) and **3a** (pink, PDB ID 5D1S), illustrating that alkylation at the sulfonamide nitrogen abolishes the key hydrogen bond to Tyr728.

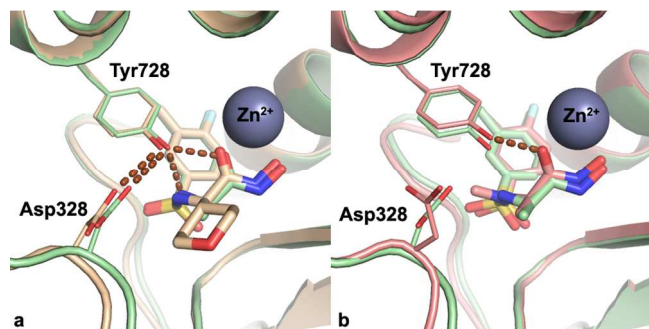


Table of Contents Graphic

